Research Article

Anjali Shivappa Baragi, Bhagyashri Gurumurthy Machul, Manohar Dhadesugur Krishnamurthy, Ramesha Adiveppagoud Patil, Anusha Vadde, Sulake Nagaraja Rao*

# Enhancing the wireless power transfer system performance and output voltage of electric scooters

https://doi.org/10.1515/EHS-2023-0136
received October 19, 2023; accepted May 06, 2024

**Abstract:** Wireless power transfer (WPT) has emerged as a groundbreaking technology that enables the transmission of electrical energy without the need for physical wires. WPT has the potential to revolutionize the charging infrastructure of electric scooters, providing a convenient and efficient method for charging the battery without using wires. This study provides an overview of the application of WPT in electric scooters, exploring the benefits, challenges, and future prospects of this technology. The study then delves into the underlying principles of WPT, including magnetic resonance and inductive coupling, which allow for efficient power transfer between the charging infrastructure and the scooter's onboard receiver. In conclusion, WPT holds great promise for electric scooters by enabling convenient and efficient charging methods. With ongoing advancements in technology and growing interest in sustainable transportation, WPT has the potential to transform the charging infrastructure of electric scooters, contributing to a cleaner and more convenient urban mobility ecosystem.

*** Corresponding author: Sulake Nagaraja Rao**, Department of Electrical Engineering, M S Ramaiah University of Applied Sciences, Bangalore, India, e-mail: nagarajarao.ee.et@msruas.ac.in
**Anjali Shivappa Baragi:** Department of Electrical Engineering, M S Ramaiah University of Applied Sciences, Bangalore, India, e-mail: 19etee003002@msruas.ac.In
**Bhagyashri Gurumurthy Machul:** Department of Electrical Engineering, M S Ramaiah University of Applied Sciences, Bangalore, India, e-mail: 19etee003004@msruas.ac.In
**Manohar Dhadesugur Krishnamurthy:** Department of Electrical Engineering, M S Ramaiah University of Applied Sciences, Bangalore, India, e-mail: 19etee003020@msruas.ac.In
**Ramesha Adiveppagoud Patil:** Department of Electrical Engineering, M S Ramaiah University of Applied Sciences, Bangalore, India, e-mail: 19etee003033@msruas.ac.In
**Anusha Vadde:** Department of Electrical Engineering, M S Ramaiah University of Applied Sciences, Bangalore, India, e-mail: anushav.ee.et@msruas.ac.in

**Keywords:** wireless power transfer, electrical scooters, electromagnetic induction, magnetic resonance

## 1 Introduction

Wireless power transfer (WPT) is one of the probable technologies for wirelessly sending electric energy from a transmitter to a receiver. Due to its numerous advantages over wired connections, WPT is a preferred option for many industrial applications. Some benefits include the absence of wires, simple charging, and quick power transmission even in bad environmental conditions (Xie et al. 2013). Nicola Tesla, around the end of the nineteenth century developed the WPT technology. He created a wireless lightbulb that could transfer the electrical charge wirelessly. Tesla employed a pair of closely spaced metal plates. The bulb was activated by passing a high-frequency AC voltage between these two plates. WPT technology, however, encountered a few problems. One of the main issues is the influence that increasing distances have on the minimal power density and low transfer efficiencies (Xie et al. 2013). As a result, WPT technology performs incredibly slowly. WPT technology has been enhanced as a result, and “strongly coupled” coils are now utilized while charging wirelessly at a distance greater than 2 m. Both capacitive power transfer (CPT) and inductive power transfer (IPT) are critical WPT technologies. While CPT is only suitable for low-power applications with very short air gaps of $10^{-4}$ to $10^{-3}$ m (Sun et al. 2018), IPT can be used for enormous air gaps of several metres and has a far more considerable output power than CPT (Sun et al. 2018).

In order to improve the power transfer efficiency and look into methods for magnetic resonance coupling, research is still being done on all WPT technologies (Oluwaferanmi Adewuyi 2022, Zakerian et al. 2019). Many more ambitious initiatives are being developed in addition to the idea of walking into a room with WPT capability and having one’s

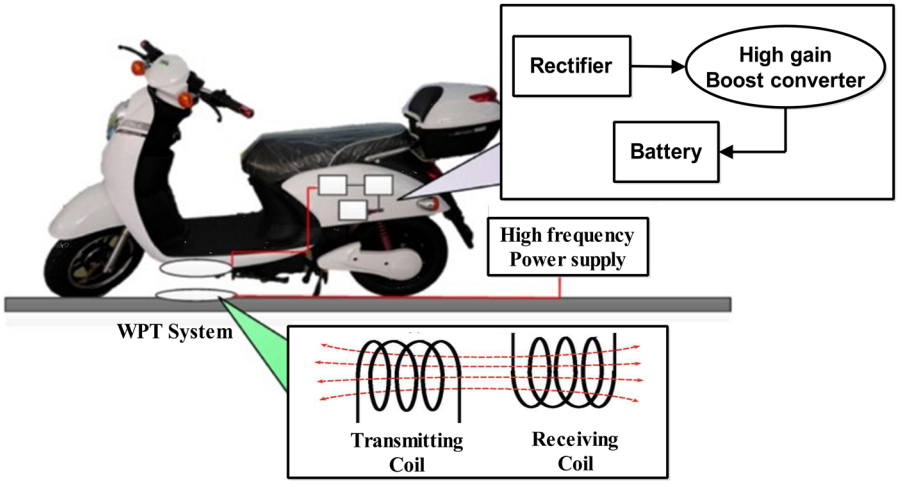


**Figure 1:** WPT for the E-scooter.

electronics automatically charge. The well-known double-decker buses of London and the bus systems in South Korea, Utah, and Germany (Sun et al. 2018) will all use wireless charging. Buses powered by electricity are growing in popularity. With the help of WiTricity, a technology created by MIT researchers, electric vehicles can wirelessly charge the electronic devices of persons traveling in such vehicles as well as the vehicles. Naturally, Qi charging is utilized Unquestionably, this wireless technology may help speed up car charging compared to plug-in methods. Wireless powering for drones is possible, thanks to the experimental technique proposed by Sun et al. (2018). The schematic diagram of the proposed WPT for the E-scooter has been shown in the Figure 1.

Additionally, as already mentioned, the possibility of employing WPT in conjunction with space-based solar panels to partially meet Earth's energy demands is the subject of continuing research and development (Cheon et al. 2010). Without the need for wires or cables, wireless communication is the transmission of energy over short or long distances (Khan-ngern and Zenkner 2014, Vadde and Sudha 2018). Wireless activities, which are simply not feasible with cables, enable services like long-range communications. The technique of delivering electric current from a power source to an electrical load without the use of connecting wires is known as wireless energy transfer, sometimes known as WPT (Cheon et al. 2010). Wireless communication is advantageous when connecting wires is difficult, risky, or impossible. In contrast to wireless telecommunications like radio, the condition for transmitting wireless power is different (Xie et al. 2013).

## 2 Background theory

WPT technology has gained significant attention in recent years as a convenient and efficient method for charging electric devices without the need for physical connectors or cables. While the concept of WPT has been around for over a century, it has seen advancements and applications in various fields, including electric scooters (Musavi and Eberle 2014, Musavi et al. 2012).

Nicola Tesla started WPT research near the end of the nineteenth century. He stated, "This energy will be collected everywhere on Earth, preferably in modest quantities, ranging from a fraction of one to a few horse-power." Remote house lighting will be one of its main uses. Tesla constructed an enormous coil attached to a tower that was 200 ft tall and had a 3 ft-diameter ball placed on top of it (Bi et al. 2016). The Tesla Tower was the name of the contraption. Tesla supplied the coil with 300 kW electricity, resonating at a frequency of 150 kHz. The top sphere's radiofrequency (RF) peaked at 100 MV. Unfortunately, the experiment failed since the 150 kHz, 21 km wavelength radio waves employed for transmission scattered in all directions (Musavi and Eberle 2014). It was a wide-beam WPT similar to a broadcasting system. Wireless communications and remote sensing have dominated the history of radio waves since Tesla's original WPT experiment. Percy L. Spencer developed the first microwave oven in the 1940s after learning about microwave heating (GHz order radio waves). At the same time, he developed a microwave radar for distant sensing. The growth of the broadcasting system led to energy harvesting from ambient radio waves, much as the microwave oven was created. Germanium radio is the most well-known use of energy harvesting from background radio waves. The radio does not require a battery to operate. It takes in radio waves for broadcasting and for electricity. In addition to ambient radio waves, other weak power sources that are all around us, such as vibration, heat, and electric light, can be used for energy harvesting (Madigan et al. 1992).

In the twenty-first century, there are more scientific publications published, and recently some significant global

research programmes have begun. Internet of Things (IoT) applications are driving recent advancements in energy harvesting. An IoT device typically uses very little power, and billions of IoT devices are anticipated. An IoT gadget has qualities that make it appropriate for energy harvesting. Among those that support RF energy harvesting is the University of Washington, which put up the idea of a wireless identification and sensing platform (WISP) (Madigan et al. 1992). UHF RFID (ultrahigh-frequency RF identification) readers are used to power and read the WISP family of sensors (Xiao et al. 2016). WISPs make use of the reader's RF signal's gathered power. They created a battery-free phone based on WISP technology that operated by mixing analog and digital methods and used only 3.48 μW electricity (Ramkumar et al. 2022). The low power of RF energy harvesting is a disadvantage. For instance, only a few W/m$^2$ power density has been measured for mobile phones and TV transmitting waves in Japan. The benefit of RF energy harvesting is that it does away with the requirement for a strong transmitter. It might be used as a far-field WPT system though, if the user needs additional strength. Wide-beam WPT was built on the basis of RFID technology (Musavi and Eberle 2014). Compared to RFID, wide-beam WPT is far more flexible. Wide-beam WPT systems are typically referred to as far-field (Fraunhofer region) WPT systems since they may provide wireless power to lots of users without detecting targets nearby. The RF power that is being transferred is used for the battery's ambient wireless charging. Radio regulations require that RF power and RF information normally come from separate RF sources. However, a more practical method, simultaneous wireless information and power transfer, has just been developed (Madigan et al. 1992).

## 3 System design

The block diagram of development of a wireless charging battery for electric scooters is shown in Figure 2, which consists of three systems, i.e. a primary system, a WPT system, and a secondary system, which carry out the power from supply to the DC load (Hu et al. 2018). The input to the primary system's rectifier, which converts AC to DC, is an AC supply. A 5-level diode-clamped inverter, also known as a multilevel inverter, is recommended in place of an inverter. This inverter lowers the system's total harmonic distortion (THD) factor and converts DC to AC with multiple-level output waveforms (Skorvaga et al. 2021).

In a WPT system, a transmitter and reception coils are the main components. AC current powers the transmitter coil to create a magnetic field, resulting in the receiving coil produces a voltage. The AC current intensifies a copper wire in the TX (transmitter) segment, creating a magnetic field. A magnetic field can cause the AC current to flow through a receiving coil, or RX, when it is placed in close proximity to one. With the transmitter (primary) and receiver (secondary), which are separated by a significant distance, power transmission is possible (say 3 cm) (Skorvaga et al. 2021).

In the secondary system circuit, three converters for transfer of power are utilized, i.e. the secondary compensation circuit, rectifier, and high-gain boost converter instead of the conventional boost converter because the output of the multilevel inverter must be increased quadruple times. Therefore, a quadratic boost converter is recommended. The power transferred by WPT is given to the secondary compensation circuit, which filters the signals from WPT, and it is given to the rectifier, which converts AC to DC; the high-gain boost con-

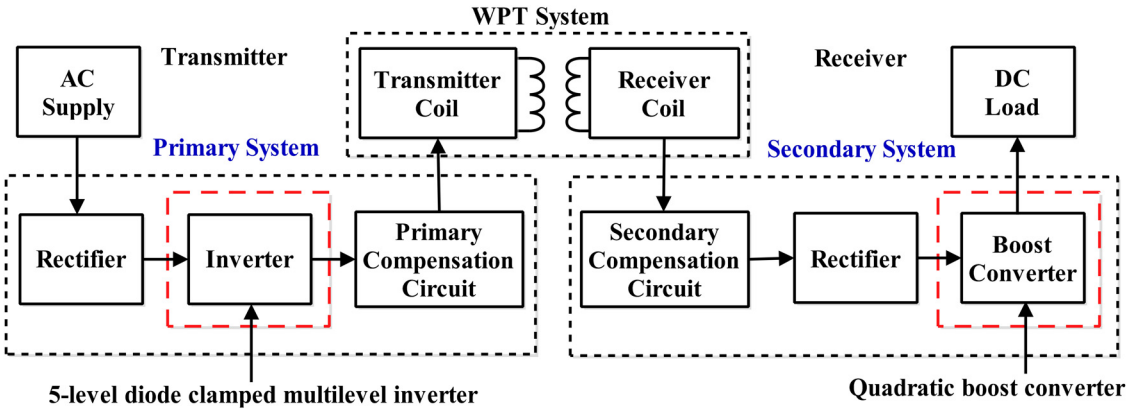


**Figure 2:** Block diagram of development of a wireless charging battery for electric scooters.

verter then steps up the DC power, and it is then given to the scooter's DC load (Skorvaga et al. 2021).

## 3.1 Rectifier

A full-wave bridge rectifier converts AC to pulsating DC, and additional filtering is usually required to smooth out the output and make it suitable for most electronic devices. To do this, a capacitor is often connected across the load. The capacitor serves as a filter, reducing the ripple voltage, and supplying a more steady DC voltage (Hu et al. 2018). The full-wave bridge rectifier does not need a centre-tapped transformer, in contrast to a centre-tapped rectifier. It can utilize a standard transformer, simplifying the circuit design and reducing the cost. The full-wave bridge rectifier has a higher output voltage and a smoother DC output than a half-wave rectifier (Liserre et al. 2005).

A filter circuit in a linear power supply known as a capacitor-input filter has a capacitor as its initial component and is connected in parallel to the rectifier's output. In this setup, the capacitor lowers the ripple voltage components while raising the output's DC voltage. As shown in Figure 3, it gives the idea about the full-wave bridge rectifier simulation model. Here, four diodes are used to convert the AC input signal to the DC input signal (Cecati et al. 2003).

## 3.2 5-level diode-clamped multilevel inverter

A high-frequency converter that converts DC produces AC. This high-frequency converter provides a frequency that is sufficient for WPT to function (Khajehoddin et al. 2007). There is DC power input. The application determines the value of the input voltage. While some applications only need 12 V, others may need thousands of volts of very high power. The high-frequency inverter is also known as the "multilevel inverter"; it is an improved alternative device to the regular two-level inverters, and it provides a desired alternating voltage level at the output. The multilevel inverter can operate at both fundamental and high-switching frequency pulse width modulations (Barkati et al. 2008).

An electronic power tool called an inverter transforms DC voltage into AC voltage. Another name for an inverter is a neutral-point-clamped or diode-clamped multilevel inverter. It is capable of producing AC voltage with multiple levels or waveforms. It is commonly employed in high-power applications such as motor drives and renewable energy systems (Barkati et al. 2008). The diode-clamped multilevel inverter offers several advantages: reduced THD, improved power quality, lower electromagnetic interference, and ability to handle high-power applications efficiently. However, it requires more complex control algorithms and additional components compared to conventional two-level inverters (Pan et al. 2005). In this article, a 5-level diode-clamped multilevel inverter (Pan et al. 2005) is employed, while it can also be performed at three, five, and nine levels.

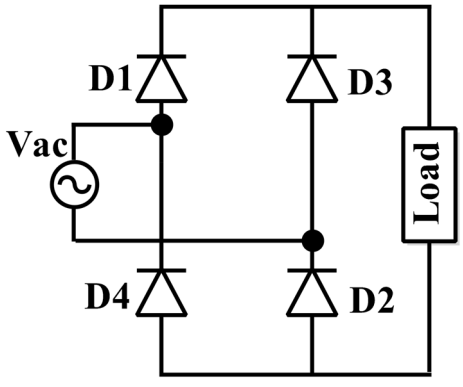


**Figure 3:** Schematic diagram of the rectifier.

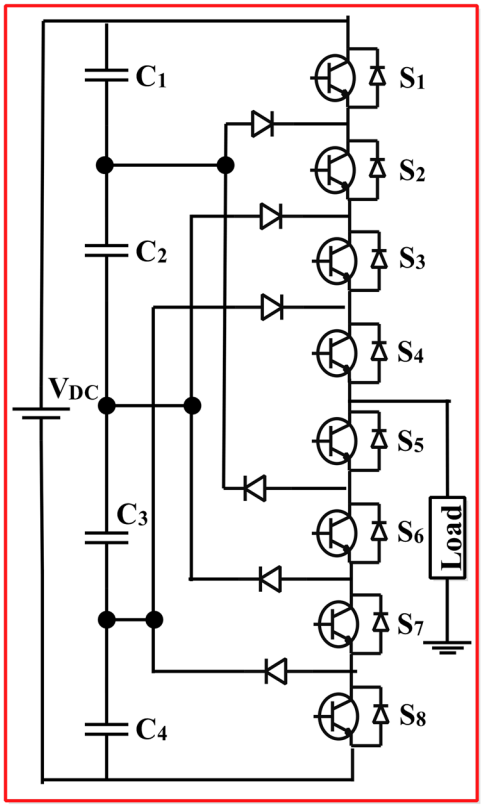


**Figure 4:** Schematic diagram of the 5-level diode-clamped multilevel inverter.

**Table 1:** Switching states of diode-clamped multilevel inverter

| Voltage ($V_0$) | On state switches |
|---|---|
| $\frac{V_{dc}}{2}$ | S1, S2, S3, S4 |
| $\frac{V_{dc}}{4}$ | S2, S3, S4, S5 |
| 0 | S3, S4, S5, S6 |
| $\frac{V_{dc}}{2}$ | S4, S5, S6, S7 |
| $\frac{V_{dc}}{4}$ | S5, S6, S7, S8 |

**Table 2:** Design specifications of a high-frequency inverter

| Parameters | Values |
|---|---|
| Input voltage | 311.7 V |
| Resistance | 20 Ω |
| Capacitors | 1 F |
| Switching frequency | 10 kHz |
| Time period | 0.1 ms |

A representation of the 5-level diode-clamped multilevel inverter is provided in Figure 4. Here, to convert the DC input signal to the AC output signal, four capacitors, six diodes, and eight switches are used (Savitha and Nagaraja Rao 2022). Table 1 gives details of the switching states of an diode-clamped multilevel inverter to obtain various levels.

The balancing of capacitors in a multilevel inverter is done by considering the symmetrical switching sequence based on the equal-phase method. However, for the higher levels, i.e. for more than 5-level inverter circuits, an additional control circuit is recommended to balance the voltage across the capacitors. Design specifications of a high-frequency inverter are specified in Table 2.

## 3.3 Transmission and receiver coils

The circular spiral design of the transmission and receiver coils is shown in Figure 5. The inner and outer diameters of the coils are 20 and 80 mm, respectively. The thickness of the spiral coil is 5 mm with the number of turns of 10. The spacing between the turns is 0.7 mm.

The magnetic flux distribution is analysed between the transmitter and receiver coils and is shown in Figure 6. The flux distribution is analysed at 410 kHz frequency and with an efficiency of 62%. The colour bar stands for the strength of the magnetic flux between the coils, and streamlines notify the direction of magnetic flux lines within the coils.

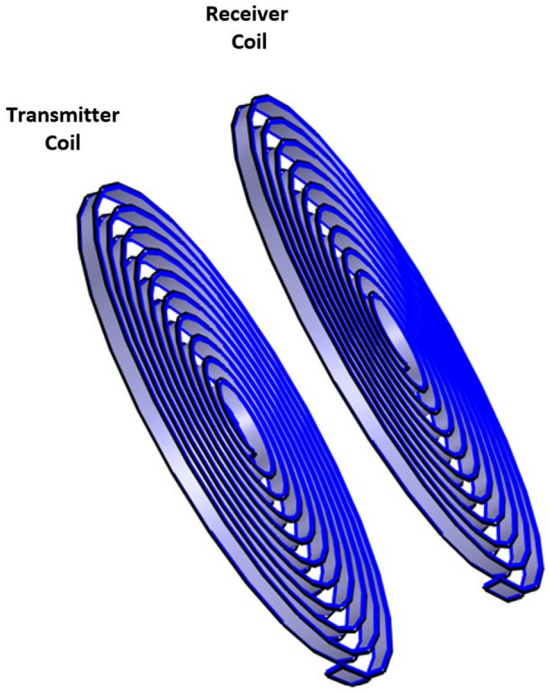


**Figure 5:** Design of transmission and receiver coils.

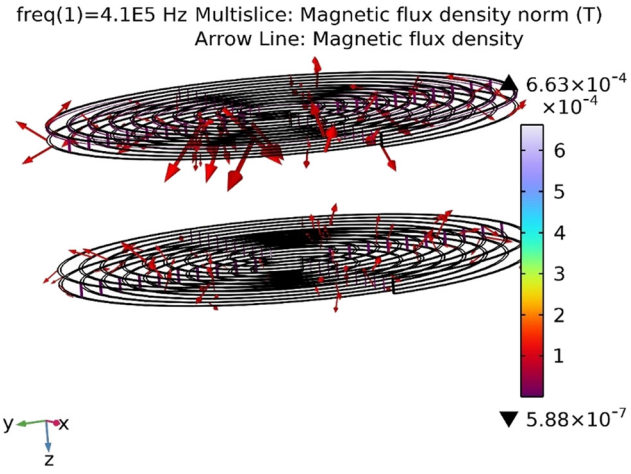


**Figure 6:** Magnetic flux distribution analysis between transmission and receiver coils.

## 3.4 Quadratic boost converter

A quadratic boost converter topology has been designed for the high conversion ratio (DC-to-DC conversion) in PV systems. The design incorporates an active zero-voltage switching snubber circuit (Silva et al. 2009). The snubber circuit protects the gadget, which also provides smooth switching. However, employing the lowest stored energy

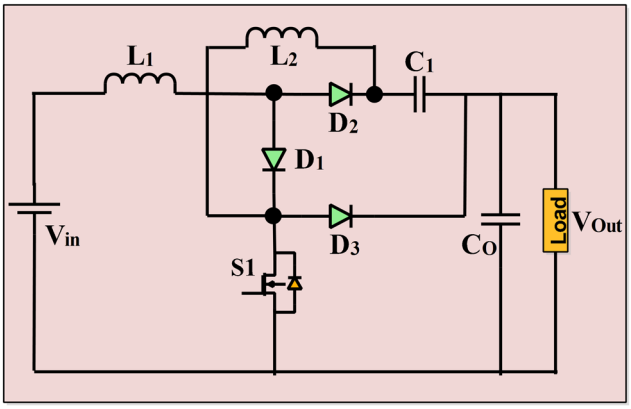


**Figure 7:** Circuit diagram of the quadratic boost converter.

technique can decrease the converter size. Conventional quadratic boost converter topologies demand a higher quantity of stored energy to be available in the capacitors utilized (Morales-Saldaña et al. 2014). A non-isolated quadratic boost converter that features a low-output-voltage ripple with respect to traditional boost converters. This advantage is in contrast with other topologies that the quadratic boost converter shows a significantly smaller output-voltage ripple with capacitors of the same capacitance. Therefore, a quadratic boost converter requires the capacitors with low-voltage ratings.

Using a quadratic boost converter shown in Figure 7, it is feasible to step up a low-voltage input to a higher-voltage output. Another name for it is a quadratic synchronous boost converter, and it is a variant of the classic boost converter (Rosas-Caro et al. 2012, Veerabhadra and Nagaraja Rao 2024).

The quadratic boost converter with a single switch is a version of the standard boost converter that makes use of modified active and passive switches. In this model, the transistor switch S and diode $D_1$ are swapped out for corresponding current sources, while the diodes $D_2$ and $D_3$ are swapped out for voltage sources. These modifications enable a more comprehensive analysis of the quadratic boost converter with a single switch. It is commonly used in various applications, including power supplies and renewable energy systems (Rosas-Caro et al. 2012).

### 3.4.1 Quadratic boost converter has two modes of operation

The Figures 8 and 9 demonstrate the quadratic boost converter circuit topologies for mode-1 and mode-2 operation, respectively.

**Mode-1:** Capacitors $C_1$ and $C_2$ are assumed to be of substantial value so that the voltage across them is practically constant over the course of a switching period, assuming that the switch S operates in an ideal manner. $D_1$ is forward-biased when switch S is activated, whereas $D_2$ and $D_3$ are reverse-biased. $V_{\text{in}}$ and $C_1$, respectively, supply current to $L_1$ and $L_2$ (Choudhury and Nayak 2015).

In mode-1 state, $I_{L1}$ and $I_{L2}$ are increased by the amount defined by

$$(\Delta I_{L1})_{\text{ON}} = \frac{V_{\text{S}} \times D \times T}{L_1}, \tag{1}$$

$$(\Delta I_{L2})_{\text{ON}} = \frac{V_{\text{S}} \times D \times T}{L_2}. \tag{2}$$

**Mode-2:** In this case, $D_1$ is reverse-biased, whereas $D_2$ and $D_3$ are forward-biased. To $C_1$ and $C_2$, respectively, chargers $L_1$ and $L_2$ are applied. $I_{L1}$ and $I_{L2}$ are lowered in this state (Choudhury and Nayak 2015).

In mode-2 state, $I_{L1}$ and $I_{L2}$ are decreased, and they are expressed by

$$(\Delta I_{L1})_{\text{OFF}} = \frac{(V_{\text{in}} - V_{C1}) \times (1 - D) \times T}{L_1}, \tag{3}$$

$$(\Delta I_{L2})_{\text{OFF}} = \frac{(V_{C1} - V_{\text{O}}) \times (1 - D) \times T}{L_2}. \tag{4}$$

Hence, the output voltage from mode-1 and mode-2 operations is

$$V_{\text{o}} = \frac{V_{\text{S}}}{(1 - D)^2}. \tag{5}$$

The inductor $L_1$ is selected as per the following formula:

$$L_1 = \frac{DV_{\text{S}}}{2F_{\text{S}}\Delta \text{I}_{L1}}, \tag{6}$$

$$I_{L1} = \frac{I_{\text{o}}}{(1 - D)^2}. \tag{7}$$

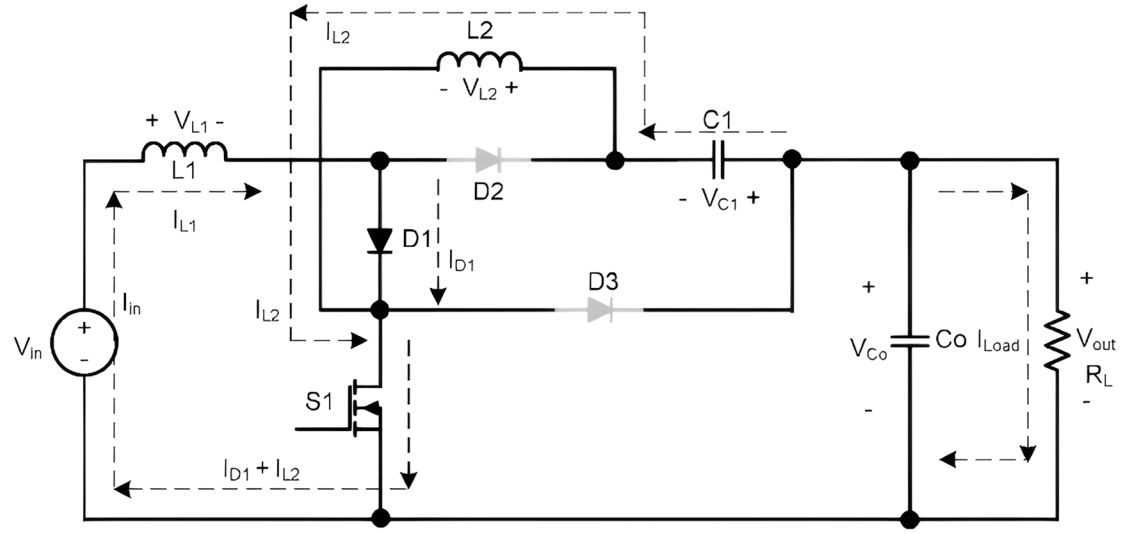


**Figure 8:** Circuit diagram for mode-1 operation of the quadratic boost converter.

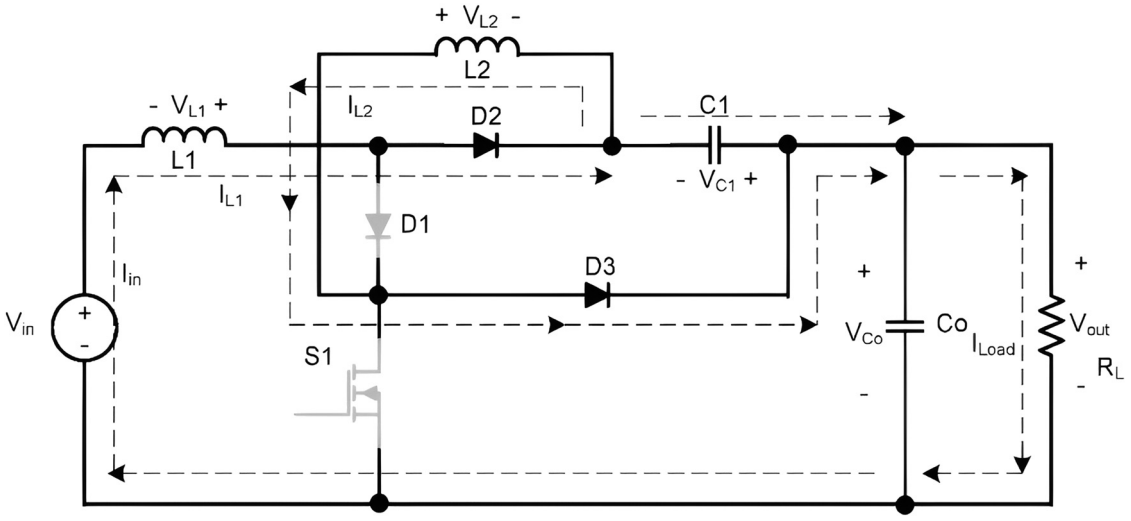


**Figure 9:** Circuit diagram for mode-2 operation of the quadratic boost converter.

The inductor $L_2$ is selected as per the following formula:

$$L_2 = \frac{DV_S}{2F_S\Delta I_{L2}}, \tag{8}$$

$$I_{L2} = \frac{I_o}{(1-D)}. \tag{9}$$

The capacitor $C_1$ is selected as per the following formula:

$$C_1 = \frac{I_o D}{(1-D)\Delta V_{C1} F_S}, \tag{10}$$

$$V_{C1} = \frac{V_S}{(1-D)}. \tag{11}$$

The capacitor $C_2$ is selected as per the following formula:

$$C_2 = \frac{I_o D}{\Delta V_{C2} F_S}, \tag{12}$$

$$V_{C2} = \frac{V_{C1}}{(1-D)}, \tag{13}$$

where $D$ is the duty ratio, $L_1$ is the inductor-1, $L_2$ is the inductor-2, $C_1$ is the capacitor-1, $C_2$ is the capacitor-2, $V_S$ is the source voltage, $F_S$ is the switching frequency, $I_{L1}$ is the current across inductor-1, $I_{L2}$ is the current across inductor-2, $\Delta I_{L1}$ is the change in the current across inductor-1, $\Delta I_{L2}$ is the change in the current across inductor-2, $I_O$ is the output current, $V_O$ is the output voltage, $V_{C1}$ is the voltage across capacitor-1, $V_{C2}$ is the

voltage across capacitor-2, $V_{C1}$ is the voltage change across capacitor-1, and $V_{C2}$ is the voltage change across capacitor-2 (Choudhury and Nayak 2015).

### 3.5 Design of the quadratic boost converter

The inductor and capacitor values of the quadratic boost converter (Angalaeswari 2021) are calculated by considering the 50 kHz switching frequency using equations (14)–(17).

$$L_1 = \frac{V_o(1-D)^2 \cdot D}{\Delta I_{L1} \cdot f_{sw}}, \tag{14}$$

$$L_2 = \frac{V_o(1-D) \cdot D}{\Delta I_{L2} \cdot f_{sw}}, \tag{15}$$

$$C_1 = \frac{I_o \cdot D}{f_{sw} \cdot (1-D) \cdot \Delta V_{C1}}, \tag{16}$$

$$C_0 = \frac{I_o \cdot D}{f_{sw} \cdot \Delta V_{C1}}. \tag{17}$$

Therefore, the designed values of $L_1$, $L_2$, $C_1$, and $C_0$ are 72.115, 114.02 µH, 86.7, and 21.69 µF, respectively.

## 4 Results

This section focuses on presenting the simulation results of individual circuits involved in the WPT system. These circuits include the primary system, the WPT system, and the secondary system. Each circuit comprises components such as a transmitter side rectifier, a 5-level diode-clamped multilevel inverter receiver side rectifier, and a quadratic boost converter.

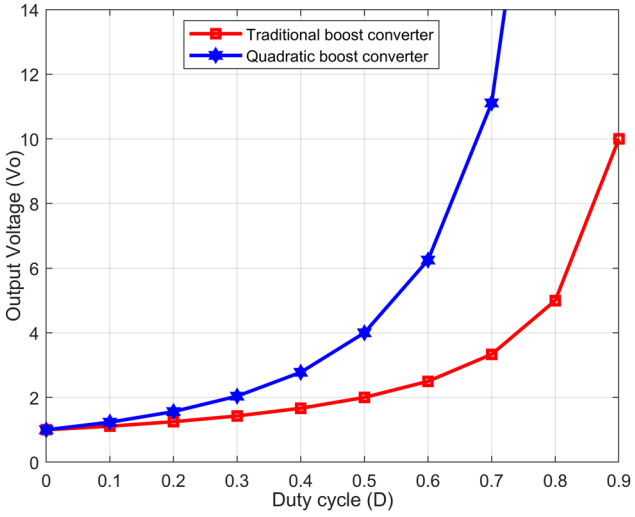


**Figure 10:** Voltage gain of conventional boost and quadratic boost converters.

The simulation aims to analyse the performance and behaviour of each circuit individually before integrating them into the complete WPT system. By studying the results obtained from these simulations, valuable insights can be gained regarding the functionality of the individual circuits.

Once the individual circuit simulations are completed, the integrated WPT circuit is then simulated using MATLAB Simulink. This integration allows for a comprehensive performance analysis of the complete WPT system. The simulation results obtained from this integrated circuit can provide a deeper understanding of the system's behaviour as a whole, including the interaction between the different components and their impact on the overall system performance.

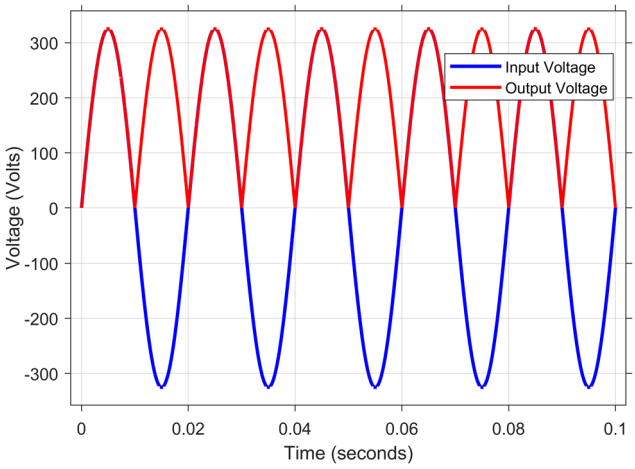


**Figure 11:** Simulation result of a rectifier showing the input and output voltage graphs as a function of time.

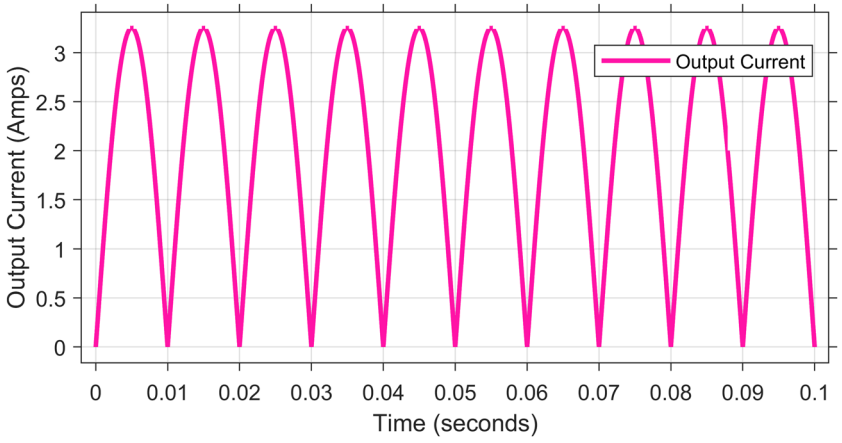


**Figure 12:** Simulation result of a rectifier showing the output current as a function of time at an AC input voltage of 325.27 V.

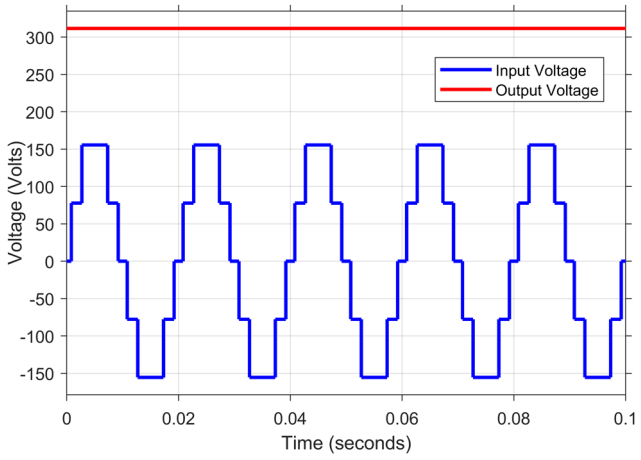


**Figure 13:** Simulated voltage result of the 5-level diode-clamped multilevel inverter.

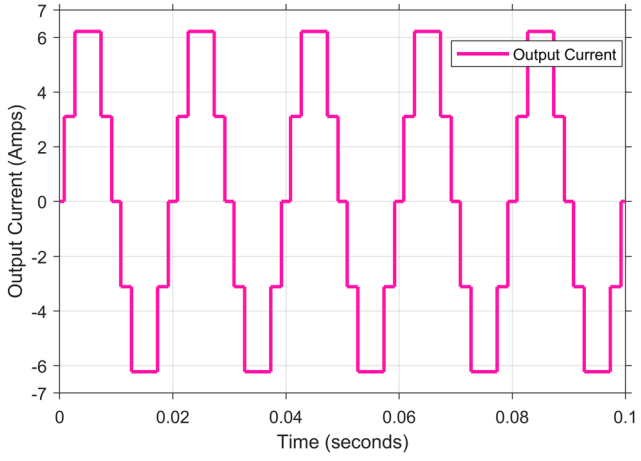


**Figure 14:** Simulated output current of the 5-level diode-clamped multilevel inverter.

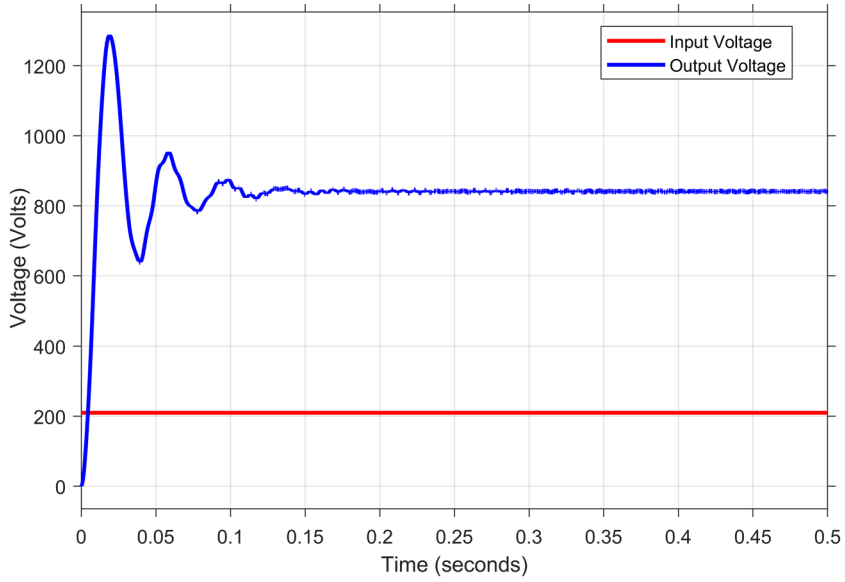


**Figure 15:** Simulation result of the quadratic boost converter.

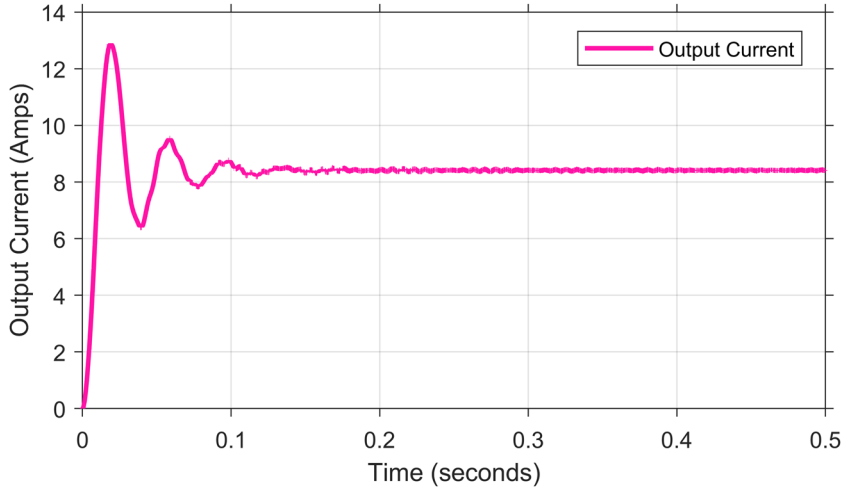


**Figure 16:** Simulated output current of the quadratic boost converter.

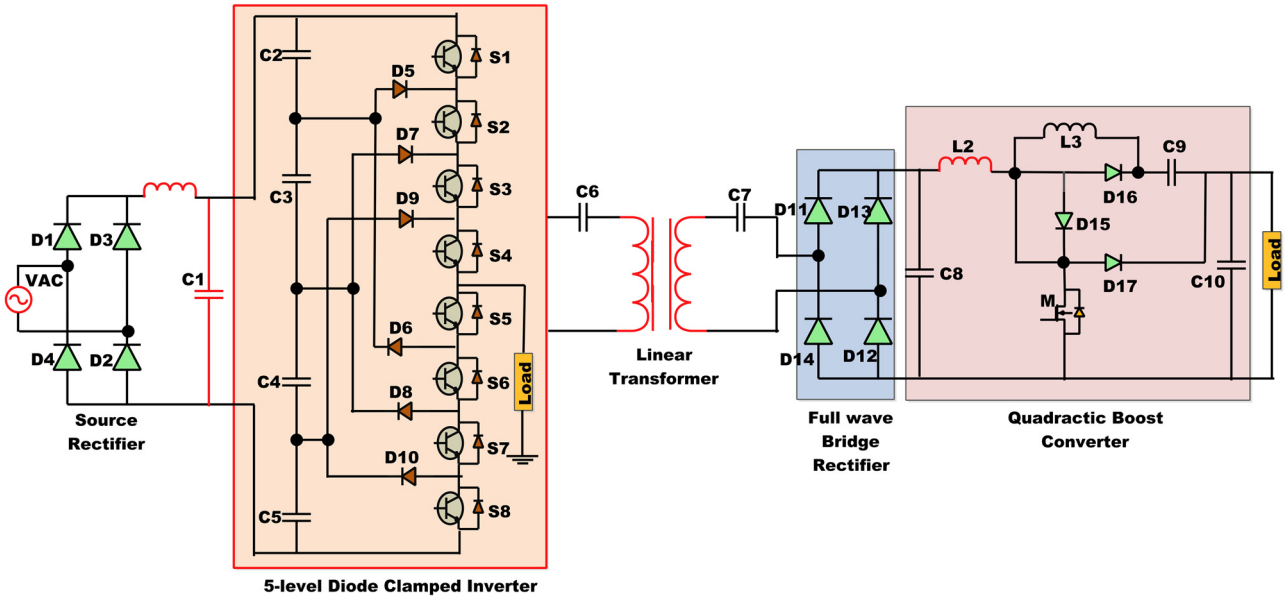


**Figure 17:** Proposed integrated circuit electric scooter.

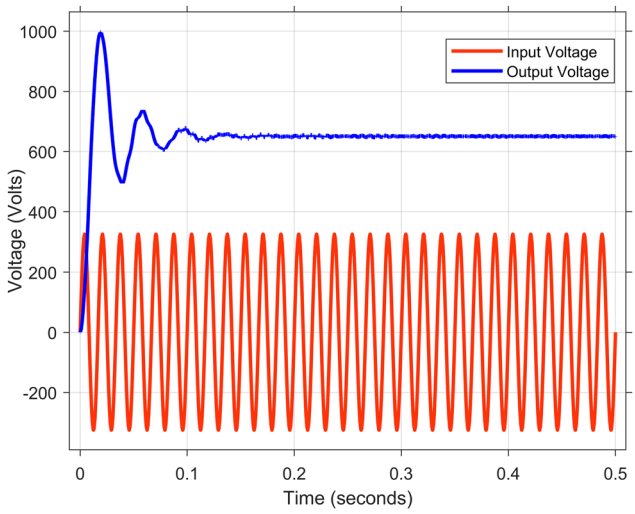


**Figure 18:** Simulation results of an integrated circuit.

## 4.1 Comparative analysis of duty cycle vs output voltage: conventional and quadratic boost converters

Figure 10 illustrates the absolute output voltage variation relative to duty-cycle variation. For a 0.5 duty cycle, the output voltage for traditional and quadratic boost converters is 2 and 4, respectively. As a result, the voltage gain for a quadratic converter is doubled for a 0.5 duty cycle, as compared to the traditional boost converter.

## 4.2 Rectifier

Figure 11 displays the input and output voltage graphs of the transmitter side of a rectifier with regard to time in seconds. At an AC input voltage supply of 325.27 V, the output current is shown in Figure 12.

**Table 3:** Comparison of the voltage, current, and THD factor of the existing and developed models

| Parameters | Existing model | Proposed model |
|---|---|---|
| Output voltage (V) | 325.22 | 650.4 |
| Output current (A) | 3.251 | 6.503 |
| THD (%) | 48.84 | 30.25 |

## 4.3 5-level diode-clamped multilevel inverter

Figure 13 illustrates the input and output voltage graphs of the high-frequency inverter's transmitter side with regard to time in seconds, where the DC input voltage supply of 311.5 V has a constant wave and the output is 155.5 V (AC voltage). Figure 14 explains about the output current graph of the transmitter side of the inverter with respect to time at an output current of 3.2 A.

## 4.4 Quadratic boost converter

Graphs of the quadratic boost converter's input and output voltages (DC–DC) with respect to time in seconds are shown in Figure 15, where the DC input voltage of 210 V has a constant wave, and the output is 840.2 V (DC voltage). Figure 16 displays the output current graph of the boost converter with respect to time at an output current of 8.381 A.

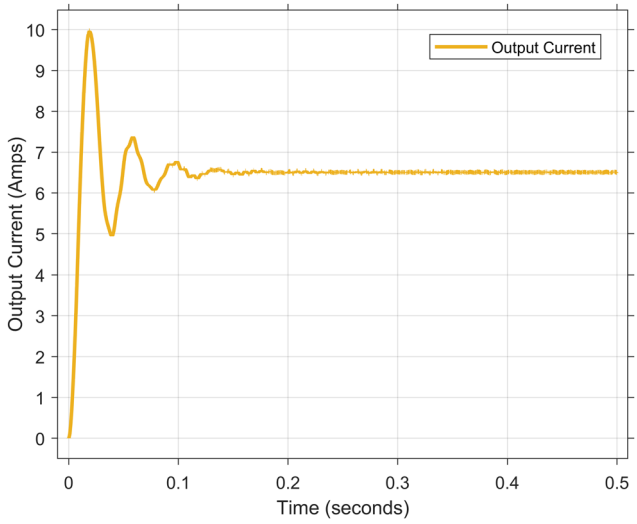


**Figure 19:** Simulated quadratic boost converter output of an integrated circuit.

## 5 Integrated circuit

From the results of each individual component, an integrated circuit can be designed in the MATLAB Simulink for the wireless power charging system for electric scooters. The overall configuration of the integrated circuit is shown in Figure 17.

From the integrated circuit, the desired output is obtained. Figure 18 explains the input and output voltage graphs of the integrated circuit with respect to time in seconds, where the AC input voltage supply of 325.27 V has the sinusoidal wave, and the output is 650.4 V (DC voltage) with a constant wave. The output voltage graph will have fluctuations in the signal until it reaches its stable condition. Figure 19 signifies the output current graph of the integrated circuit with respect to time at an output current of 6.51 A.

## 6 Comparison

Table 3 presents a comparison of the output voltage, output current, and %THD values. In the existing circuit, the output voltage is 325.22 V. However, in the created model, a quadratic boost converter is employed to enhance the output voltage by two times that of the existing circuit. Therefore, the output voltage of the model is 650.4 V. As for the output current, the present circuit has a value of 3.251 A. In contrast, the developed model has an output current of 6.503 A. It is worth noting that both the present circuit and the model are measured at the same time. The THD factor, mentioned in the table, likely indicates that the level of harmonic distortion present in the output of diode-clamped multilevel inverter is less when compared to the conventional inverter.

## 7 Conclusions

In conclusion, WPT in electric scooters offers several advantages and has the potential to revolutionize the charging process. WPT eliminates the need for physical connections or cables, making charging more convenient and user-friendly. Users can simply park their electric scooters on a charging pad or within the charging range, and the power transfer will initiate automatically. There is no direct physical contact with electrical components, reducing the chance of damage or injury during the charging process. By removing the physical wear and tear associated with traditional charging connectors, WPT can enhance electric scooters' overall durability and lifespan. Without the need for repeated plugging and unplugging, the electrical contacts and charging ports are less prone to damage. Overall, WPT in electric scooters offers an innovative and promising solution for convenient and efficient charging. With further advancements and widespread adoption, it has the potential to transform the way to charge and use electric scooters, making them more accessible and environment-friendly.

**Acknowledgements:** We thank our beloved MSRUAS Vice Chancellor and Management team for their valuable assistance and permission for publishing our research work.

**Funding information:** The authors have not received any financial assistance for this research.

**Author contributions**: All authors accepted the responsibility for the content of the manuscript and consented to its submission, reviewed all the results, and approved the final version of the manuscript. ASB and BGM helped in conceptualization, methodology and manuscript preparation. MDK and RAP worked on MATLAB simulation and writing original draft preparation. AV helped in supervision, review and editing. SNR contributed to supervision, writing, review and editing.

**Conflict of interest:** The authors declare no conflicts of interest regarding this article.

**Data availability statement:** All data generated or analysed during this study are included in this published article.

## References

Angalaeswari S. (2021). "Design and execution of quadratic boost converter (QBC) in renewabe energy synergies," *Turk. J. Comput. Math. Educ. (TURCOMAT)*, vol. 12, no. 9, pp. 2957–2968.

Barkati S., Baghli L., Berkouk E. M., and Boucherit M. S. (2008). "Harmonic elimination in diode-clamped multilevel inverter using evolutionary algorithms," *Electr. Power Syst. Res.*, vol. 78, no. 10, pp. 1736–1746.

Bi Z., Kan T., Mi C. C., Zhang Y., Zhao Z., and Keoleian G. A. (2016). "A review of wireless power transfer for electric vehicles: Prospects to enhance sustainable mobility," *Appl. Energy*, vol. 179, pp. 413–425.

Cecati C., Dell'Aquila A., Liserre M., and Monopoli V. G. (2003). "Design of H-bridge multilevel active rectifier for traction systems," *IEEE Trans. Ind. Appl.*, vol. 39, no. 5, pp. 1541–1550.

Cheon S., Kim Y. H., Kang S. Y., Lee M. L., Lee J. M., and Zyung T. (2010). "Circuit-model-based analysis of a wireless energy-transfer system via coupled magnetic resonances," *IEEE Trans. Ind. Electron.*, vol. 58, no. 7, pp. 2906–2914.

Choudhury T. R. and Nayak B. (2015, October). Comparison and analysis of cascaded and quadratic boost converter," in *2015 IEEE Power, Communication and Information Technology Conference (PCITC)*, IEEE, pp. 78–83.

Hu J. S., Lu F., Zhu C., Cheng C. Y., Chen S. L., Ren T. J., et al. (2018). "Hybrid energy storage system of an electric scooter based on wireless power transfer," *IEEE Trans. Ind. Inform.*, vol. 14, no. 9, pp. 4169–4178.

Khajehoddin S. A., Bakhshai A., and Jain P. K. (2007, June). "A voltage balancing method and its stability boundary for five-level diode-clamped multilevel converters," in *2007 IEEE Power Electronics Specialists Conference*, IEEE, pp. 2204–2208.

Khan-ngern W. and Zenkner H. (2014, March). "Wireless power charging on electric vehicles," in *2014 International Electrical Engineering Congress (iEECON)*, IEEE, pp. 1–4.

Liserre M., Blaabjerg F., and Hansen S. (2005). "Design and control of an LCL-filter-based three-phase active rectifier," *IEEE Trans. Ind. Appl.*, vol. 41, no. 5, pp. 1281–1291.

Madigan M., Erickson R., and Ismail E. (1992, June). "Integrated high quality rectifier-regulators," in *PESC'92 Record. 23rd Annual IEEE Power Electronics Specialists Conference*, IEEE, pp. 1043–1051.

Morales-Saldaña J. A., Loera-Palomo R., Palacios-Hernández E., and González-Martínez J. L. (2014). "Modelling and control of a DC–DC quadratic boost converter with R2P2," *IET Power Electron.*, vol. 7, no. 1, pp. 11–22.

Musavi F. and Eberle W. (2014). "Overview of wireless power transfer technologies for electric vehicle battery charging," *IET Power Electron.*, vol. 7, no. 1, pp. 60–66.

Musavi F., Edington M., and Eberle W. (2012, September). "Wireless power transfer: A survey of EV battery charging technologies," in *2012 IEEE Energy Conversion Congress and Exposition (ECCE)*, IEEE, pp. 1804–1810.

Oluwaferanmi Adewuyi V. (2022). "Overview and advancements in electric vehicle WPT systems architecture," in *Power Electronics, Radio Frequency and Microwave Engineering*, IntechOpen. doi: 10.5772/intechopen.106254.

Pan Z., Peng F. Z., Corzine K. A., Stefanovic V. R., Leuthen J. M., and Gataric S. (2005). "Voltage balancing control of diode-clamped multilevel rectifier/inverter systems," *IEEE Trans. Ind. Appl.*, vol. 41, no. 6, pp. 1698–1706.

Ramkumar M. S., Reddy C., Ramakrishnan A., Raja K., Pushpa S., Jose S., et al. (2022). "Review on Li-ion battery with battery management system in electrical vehicle," *Adv. Mater. Sci. Eng.*, vol. 22, pp. 1–8.

Rosas-Caro J. C., Mancilla-David F., Mayo-Maldonado J. C., Gonzalez-Lopez J. M., Torres-Espinosa H. L., and Valdez-Resendiz J. E. (2012). "A transformer-less high-gain boost converter with input current ripple cancelation at a selectable duty cycle," *IEEE Trans. Ind. Electron.*, vol. 60, no. 10, pp. 4492–4499.

Savitha M. and Nagaraja Rao S. (2022). "Switching angle optimization and fault analysis of a multistring-multilevel inverter for renewable-energy-source applications," *Clean. Energy*, vol. 6, no. 6, pp. 907–930.

Silva F. S., Freitas A. A., Daher S., Ximenes S. C., Sousa S. K., Edilson M. S., et al. (2009, September). "High gain DC-DC boost converter with a coupling inductor," in *2009 Brazilian Power Electronics Conference*, IEEE, pp. 486–492.

Skorvaga J., Frivaldsky M., and Pavelek M. (2021). "Design of a wireless charging system for e-scooter," *Elektronika ir. Elektrotechnika*, vol. 27, no. 2, pp. 40–48.

Sun L., Ma D., and Tang H. (2018). "A review of recent trends in wireless power transfer technology and its applications in electric vehicle wireless charging," *Renew. Sustain. Energy Rev.*, vol. 91, pp. 490–503.

Vadde A. and Sudha B. (2018). "Enhancement of efficiency for wireless power transfer system using wireless link," in *2018 International Conference on Circuits and Systems in Digital Enterprise Technology (ICCSDET)*, IEEE, pp. 1–6.

Veerabhadra J. and Nagaraja Rao S. (2024). "Comparative assessment of high gain boost converters for renewable energy sources and electrical vehicle applications," *Energy Harvesting Syst.*, vol. 11, no. 1, pp. 1–17, doi: 10.1515/ehs-2022-0144.

Xiao J., Cheng E., Cheung N., Zhang B., and Pan J. F. (2016, December). "Study of wireless charging lane for electric vehicles," in *2016 International Symposium on Electrical Engineering (ISEE)*, IEEE, pp. 1–4.

Xie L., Shi Y., Hou Y. T., and Lou A. (2013). "Wireless power transfer and applications to sensor networks," *IEEE Wirel. Commun.*, vol. 20, no. 4, pp. 140–145.

Zakerian A., Vaez-Zadeh S., and Babaki A. (2019). "A dynamic WPT system with high efficiency and high power factor for electric vehicles," *IEEE Trans. Power Electron.*, vol. 35, no. 7, pp. 6732–6740.